Pulsed Laser Deposition Of $YBa_2Cu_3O_{7-\delta}/PrBa_2Cu_3O_{7-\delta}$

By

Stephanie J. Recker

HBSc Brock University

A THESIS SUBMITTED IN PARTIAL FULFILLMENT OF

THE REQUIREMENTS FOR THE DEGREE OF

MASTERS OF SCIENCE

in

THE FACULTY OF MATHEMATICS AND SCIENCE

DEPARTMENT OF PHYSICS

We accept this thesis as conforming

to the required standard

.....

.....

.....

.....

.....

BROCK UNIVERSITY

January 1998

Abstract

The process of depositing thin films by the use of pulsed laser deposition (PLD) has become a more widely used technique for the growth of substances in a thin film form. Pulsed laser deposition allows for the stoichiometric film growth of the target which is of great significance in the deposition of High Temperature Superconducting materials. We will describe a system designed using an excimer laser and vaccum chamber in which thin films and superlattices of $YBa_2Cu_3O_{7-\delta}$, $PrBa_2Cu_3O_{7-\delta}$, and $YBa_2Cu_3O_{7-\delta}$/ $PrBa_2Cu_3O_{7-\delta}$ were deposited on $SrTiO_3$. Results of resistivity measurements using the four probe technique will be shown.

Acknowledgement

I would now like to take this opportunity to thank all those who have supported me over the last couple of years. I am very grateful to my supervisor, Dr. Fereidoon Razavi, for the opportunity to work with his guidance and allowing me the opportunity to develop independent research skills. His guidance and support along with understanding and patience were appreciated greatly.

To the guys in the machine shop, Roland, Tony and Grant, who were good enough to get my requests for jobs done as quick as they could. And to the guys in the electronics shop, John, Gary and Bob, who also were quick to help with me requests made and offering advice. And to John Vandenhoff for the supply of liquid nitrogen and assistance, and Frank Benko for countless times of getting me out of a jam when something was needed last minute.

To my good friends, Barry, Katarin, Julie, Mary-beth, Tara, Tracy, Nancy, Marion, Marko, Judy, Paul, Ronald and Gord - you guys have been life savors many times throughout the years and I thank you deeply for your support, patience and understanding through both the good and bad times.... At this time I would also like to thank Gail Neff, Mrs and Dr. Bown, Tim Jones, and Barb and Roger for their words of encouragement throughout my graduate studies. And finally to my family, who have supported and encouraged me throughout my studies, thanks for believing in me.

Table of Contents

List of Figures

List of Tables

Chapter 1

Introduction

The word laser is an acronym for **L***ight* **A***mplification by* **S***timulated* **E***mission of* **R***adiation*. It is considered a *pure* energy source composed of monochromatic and coherent photons. The laser may be described as an oscillator or amplifier of light waves and its narrow beam of light propagates in almost a straight line unless the beam is either reflected or refracted. Laser usage has become essential in the areas of medical technology, metallurgy and the electronics industry. For material science, lasers have come to play a substantial role as either a passive component for process monitoring or as an active tool by coupling its radiation energy into the material being processed; resulting in various applications such as localized melting during optical fiber pulling, laser annealing of semiconductors, surface cleaning by desorption and pulsed laser depostion, laser-induced rapid quench to improve surface hardening, and most recently pulsed laser deposition (PLD) for growing thin films [1] .

Film properties are enhanced by the effects of the high energy of the depositing species, often 5 to $\geq$ 100 eV, as a result of pulsed laser deposition [2]. One of the most ideal features of PLD is its capability to create a film where the film's stoichiometry is comparable to that of the targets. This is highly important when working with the *high* T_c (mixed) oxide superconductors (HTS).

The versatility of PLD is evident in the ease in which the targets are changed, compatibility with small targets, that there are no restrictions on the material (targets) used

for film deposition, and target usage is much more efficient. A useful feature is that deposition is possible in a reactive gas environment. Its most unique feature though would be that it is capable of congruent evapouration as pulse heating enables all components to be evapourated instantaneously which is beneficial when dealing with multicomponent systems.

In 1986 Bednorz and Müller [5] discovered superconductivity in a layered perovskite, $La_{2-x}Ba_xCuO_4$ (LBCO), which has a $T_C > 30K$, making LBCO the first of what are known as high temperature superconductors. Then in 1987, Wu *et. al.* [6], announced that the compound $YBa_2Cu_3O_{7-x}$ (Y123) had a $T_c \simeq 93K$ which was a major breakthrough due to this temperature being well above the boiling point of liquid nitrogen. For both theoretical and experimental reasoning, it has become common knowledge that the CuO_2 planes and their interactions are essential for the occurrence of high-T_c superconductivity. A suitable investigation of the coupling effect of the CuO_2 planes by the use of high-T_c inserted multilayers by systematically adjusting the thickness of the normal state and high-T_c superconducting material. In the low-temperature region ($<$ 100K), the resistivity of PrBCO is several orders higher than that of YBCO, thusly YBCO/PrBCO/YBCO is a hetero-epitaxially grown S/N/S system [25], enabling the variation of the strength of the interlayer coupling between the YBCO layers without changing the properties of the YBCO layers.

High-T_c superconducting multilayers of YBCO/PrBCO have been successfully constructed by several groups and their results used for comparison. A commonly observed occurrence in the multilayers is that their T_c values change with the thickness of both the YBCO and the PrBCO layers which implies the existence of the interlayer coupling between the superconducting layers. We studied the the superconductivity in $YBa_2Cu_3O_{7-\delta}/PrBa_2Cu_3O_{7-\delta}$ superlattices, because varying the thickness of either the YBCO or PrBCO layers affects the coupling strength between the YBCO layers as well

as the val ue of T_c itself. The use of $YBa_2Cu_3O_{7-\delta}/PrBa_2Cu_3O_{7-\delta}$ structuring has two main and obvious advantages:

a) PBCO has an orthorhombic structure with lattice parameters very close to that of YBCO.

b) PBCO is a nonsuperconductor with a very high resistivity at low temperatures.

The primary objective of this research was to set up the pulsed laser deposition system. Once the laser was set up and operational, focus was then turned onto the vacuum chamber, designing of the heater, target holder, substrate holder, the focusing of the laser beam, decreasing the experimental run time from 12 hours to 5 hours by replacing

the cryogenic pump with a turbo pump, optimizing the system parameters and interfacing the target rotation and laser triggering with a computer to run simultaneously. Then, once the system was operational, it was used in the process of the deposition of thin films of a heterostructure or superlattice nature using $YBa_2Cu_3O_{7-\delta}$ and $PrBa_2Cu_3O_{7-\delta}$ layers. The superlattices of YBCO and PrBCO compounds were created keeping the thickness of the yttrium layers constant and gradually increasing the thickness of the PBCO layers in between and then comparing the resistivities of these superlattices as well as trends in their behaviour to that of previously published research. Chapter two discusses the properties of thin films and some aspects of the theory underlying resistivity. The following chapter gives a description of the experimental apparatus, the optimized parameters and the procedure followed for the deposition of the films. Chapter four of this thesis contains some relevant properties of superconductivity, some semiconductivity, some discussion on the perovskite compounds and the results from films deposited with this system. The final chapter will contain some concluding remarks.

Chapter 2

Thin Films and Pulsed Laser Deposition

2.1 Thin Film

2.1.1 Overview

High temperature thin film fabrication is aimed at the fabrication of electronic device components, such as sensors or passive microwave devices (filters, delay lines) designed into stripline technology. Thin films are prepared on substrates to achieve properties not easily attainable or not attainable at all by the substrates themselves. These films are fabricated for particular properties which can be divided into five basic categories with particular applications as shown in Table 2.1 [9], [12]. It can be seen from this particular table that the applications of thin films indeed are very broad and quite often there are multiple properties that can be attained at the same time.

The thin film form of a solid material is when this material is built up as a thin layer on a solid support (substrate), continually by controlled condensation of the individual atomic, molecular or ionic species. This is done by either a direct physical process, such as the technique of pulsed laser deposition described in a later section, or via a chemical and/or electrochemical reaction. It is not just the small thickness of a thin film that its' unique and distinctive properties are attributed to, but it is actually the microstructure that results from its fabrication by the progressive addition of the basic building blocks one by one that defines the thin film [13].

High temperature thin films, when properly prepared, have properties that resemble

Table 2.1: Thin Film Applications

Thin-film property category	Typical applications
Optical	Reflective/antireflective coatings Interference filters Decoration (colour, luster) Memory discs (CDs) Waveguides
Electrical	Insulation Conduction Semiconductor devices Piezoelectric drivers
Magnetic	Memory discs
Chemical	Barriers to diffusion or alloying Protection against oxidation or corrosion Gas/liquid sensors
Mechanical	Tribological (wear-resistant) coatings Hardness Adhesion Micromechanics
Thermal	Barrier layers Heat sinks

those measured in single crystals. Presently there are two strategies used in the growth of thin films to ensure the high T_c value of the cuprate superconductor films:

i) preparation of epitaxial films

ii) preparation of highly textured bulk samples [?].

Both these methods are aimed at reducing in the number of grain boundaries through single-crystallinity and alignment of the CuO_2 planes in the most favourable direction (i.e. parallel to the transport currents).

Films can be prepared by various forms of sputtering and evapouration, but they lack the control of the composition that is more prominent in the laser ablation of sintered ceramic targets. Laser ablation is usable for a range of compounds and tends to preserve the cation composition. In all cases though, the parameters such as background pressure, substrate temperature and the partial pressure and degree of activation of the oxygen must be accurately controlled and optimized. Each system is optimized accordingly with respect to the material(s) being depostited so that the resulting film has the "best" characteristics (slope steepness, sharp normal-superconducting transition, clean uniform surface, etc..). The best films are fabricated by *in situ* annealing on a hot substrate at 750-820°C, with an oxygen flow.

2.2 Pulsed Laser Deposition

2.2.1 Features

In pulsed laser deposition, the majority of the material vapourized from the target is in the form of macroparticles rather than atoms or molecules as in the case of other vapourization techniques. One of the most ideal features of PLD is its capability to create a film where the film's stoichiometry is comparable to that of the target. This is highly important when working with the *high* T_c (mixed) oxide superconductors (HTS).

The versatility of PLD is evident in the ease in which the targets are changed, compatibility with small targets, that there are no restrictions on the material (targets) used for film deposition, and target usage is much more efficient. A useful feature is that deposition is possible in a reactive gas environment. Yet its most unique feature though would be that it is capable of congruent evapouration as pulse heating enables all components to be evapourated instantaneously which is beneficial when dealing with multicomponent systems.

2.2.2 Problems

There are two major drawbacks to PLD. One is that due to the narrow angular distribution of the plume, there is a lack of uniformity over a large area [1], that is the depositing species is confined to a small area and if the depositing area is too large the film is not deposited in a uniform thickness to the edge of the substrate. And secondly, *splashing* is considered the other major drawback, whereby the film's morphology is not uniform. Unavoidably, the PLD technique always results in particulates being present on the smooth surface of the deposited films.

2.2.3 In Situ Growth

Upon removal from the vacuum chamber, high temperature superconducting films grown *in situ* superconduct. These films are grown in a layer by layer fashion on heated substrates in the vacuum with surface diffusion playing an important role, enabling the atoms to move into their equilibrium sites. For *in situ* growth, a substrate temperature of above 700°C and an O_2 partial pressure between 1 and 50 Pa is required.

2.2.4 Substrates

A substrate that is well lattice matched, atomically flat and chemically compatible is essential for growing high-quality ultrathin films [?]. Up to approximately $1\mu m$ in thickness, high-quality thin films can be depositied having epitaxial growth on a suitable substrates. The best substrates are themselves perovskites, such as $SrTiO_3$ (with a lattice mismatch of +1.2% at deposition temperature), MgO, $NdGaO_3$, and $LaAlO_3$. MgO, with a mismatch of 8% when correctly prepared can also make a good substrate. All known substrates fall into a general ideal having the following properties:

1. a smooth, clean surface, free of twins and other structural inhomogeneities;
2. matched lattice parameters between substrate and film;
3. chemical compatibility;
4. matched coefficients of thermal expansion;
5. no phase transformations between room temperature and deposition or annealing temperatures; and
6. electrical properties, such as dielectric constant, compatible with required applications [4].

2.2.5 Heterostructures

Additional functionality in thin films can be achieved by depositing multiple layers of different materials. When alternating layers are made using nanometer thicknesses of semiconducting materials, the result is a "superlattice" that has electrical properties governed by the constructed periodicity rather than by the atomic periodicity. Thus, multilayer thin films can behave as completely new, engineered materials unknown in bulk form. When multiple layering is combined with lithographic patterning in the plane

of the films, microstructures of endless variety can be constructed. This is the basic technology of the integrated circuit industry, and more recently it is being applied to optical waveguide circuitry and to micromechanical devices [12].

2.3 Resistivity

As mentioned previously in both the introduction and chapter 2, the electrical resistivity of a compound, or more readily the absence of electrical resistance below a critical temperature, is one of the defining characteristics of a superconducting material. Resistivity is considered an important material parameter that is closely related to the carrier drift; it is a measure of the materials natural resistance to current transport. It is considered to be a *normalized* resistance that does not depend on the physical dimensions of the material.

In most materials, the relationship between the voltage resulting across an object, (V_2 - V_1), and the applied current can be sufficiently represented by the linear relation of Ohm's law:

$$R = \frac{V}{I} \tag{2.1}$$

The resistance R is a function of both the material and the shape of the object. However, the resistivity ρ is only a property of the material, specifying how much the material hinders the motion of the charge. In terms of this concept, the resistance R of a length L of a material over a constant cross-sectional area A is given by.

$$R = \frac{\rho L}{A} \tag{2.2}$$

The linear relationship of Ohm's law follows from the assumption that a material's resistivity is independent of the applied voltage or current.

2.3.1 Electrical Conductivity

The existence of a potential difference between two points on a material as a result of an applied current establishes an electric field E along this axis resulting in an acceleration of the electrons from the force exerted on them by the electric field.

$$\mathbf{F} = -eE = m\left[\frac{dv}{dt}\right] \tag{2.3}$$

where over time t that is within the order of collision time τ, the electrons have an average velocity

$$v = -\frac{eE}{2m}\tau. \tag{2.4}$$

The current density J is then

$$\mathbf{J} = nev_{av} = \frac{ne^2\tau}{m}\mathbf{E}. \tag{2.5}$$

The dc electrical conductivity is defined by Ohm's law so that

$$\mathbf{J} = \sigma\mathbf{E} = \frac{1}{\rho}\mathbf{E}. \tag{2.6}$$

2.3.2 Electron-Phonon Interaction

The supercurrent is a result of the formation of Cooper pairs of electrons, and for most superconductors the mechanism that is responsible for the formation of these Cooper pairs is the electron-phonon interaction. For normal metals, the periodicity of the lattice is disturbed by thermal vibrations (phonons) that interact with the conduction electrons causing them to scatter. With the disturbance of the conduction electron flow that is caused by the phonons, the electrical conductivity is inversely proportional to the temperature. That is:

$$\sigma \propto \frac{1}{T} \tag{2.7}$$

or

$$\rho \propto T. \tag{2.8}$$

For finite but low temperatures, $T < \Theta_D$, the relaxation time τ has the limiting temperature dependence of $\tau \approx T^{-3}$. For even lower temperatures though, there is a more dominant scattering in the forward direction that introduces another T^2 factor resulting in the limiting behaviour of Bloch's T^5 law:

$$\rho \propto T^5 \qquad\qquad T < \Theta_D. \tag{2.9}$$

The electrical conductivity of metals when at absolute zero is a result of the presence of impuritie, defects and deviations of the background lattice of positive ions from the condition of perfect periodicity [10].

$$\rho \propto \rho_{imp} \qquad\qquad T = 0 \tag{2.10}$$

2.3.3 Resistivity

Lattice defects, impurity atoms and other imperfections within a metallic conductor also contribute to the scattering of the electrons moving through the material. An upper-limit on the overall electrical conductivity of the metal results from the temperature-independent contributions of these impurities.

The conductivities arising from the impurity and phonon contributions, according to Matthiessen's rule, add as reciprocals resulting in a total resistivity

$$\rho(T) = \rho_o + \rho_{ph}(T) \tag{2.11}$$

where the phonon term ρ_{ph} is proportional to T at high temperatures and to T^5 via the Bloch law, Eq 2.9, at low temperatures. This implies that for temperatures above room

temperature, the impurity contribution, ρ_o, is negligible and

$$\rho(T) \approx \rho(300K)\left[\frac{T}{300K}\right] \qquad 300K < T. \tag{2.12}$$

At low temperatures, far below the Debye temperature, the Bloch T^5 law applies to give [10]

$$\rho(T) = \rho_o + AT^5 \qquad T \ll \Theta_D. \tag{2.13}$$

From equations 2.13 and 2.12, the temperature coefficient of resistivity is evidentally positive for metals which is why they become better conductors at low temperatures. Yet for semiconductors there is a decrease in the number of mobile charge carriers that result from the return of thermally excited conduction electrons which inturn results in an increase in resistivity with decreasing temperature implying a negative temperature coefficient [10].

2.4 Semiconductivity

A vast majority of the solid state devices present in the market are constructed from a class of materials known as semiconductors. Semiconductors are the intermediate case between insulators and metals. An insulator is characterized by its very wide energy band gap, as shown in Figure 2.1 (a). The thermal energy available at room temperature excites very few electrons in these wide band gap materials from the valence band into the conduction band. This results in very few carriers and therefore the material is a poor conductor of current. In the case of metals, the band gap is either very small or non-existent due to an overlap of the valence and conduction bands. This results in an abundance of carriers, and thus metals are excellent conductors of current. For semiconductors thermal energy causes an excitation of electrons from the valence band

into the conduction band creates a moderate number of carriers thus giving rise to a current-carrying capability somewhere between poor and excellent [14].

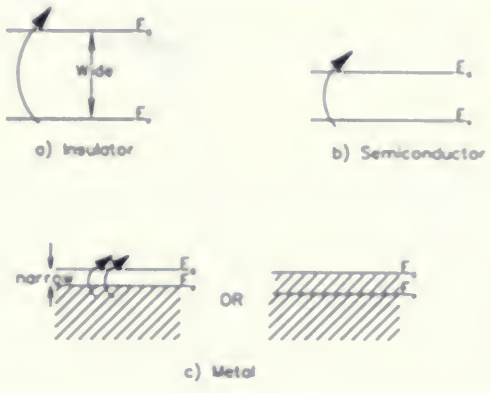

Figure 2.1: Explanation of the distinction between a) insulators, b) semiconductors - where thermals excitation is moderately easy, and c) metals using the energy band model.

2.5 Transition Temperature

In theory, the transition of a material from the normal to the superconducting state is very sharp, however, experimentally this transition can be either very abrupt or more gradual. A measure of the purity or quality of the sample material is the sharpness in the transition drop to zero. In the case of high-temperature superconductors, doping of paramagnetic ions at the copper sites causes the transition to both shift to lower temperature, and to broaden in its width. The doping of the yttrium sites though in $YBa_2Cu_3O_{7-\delta}$ tends to have little effect on T_c. The delocalization of the superelectrons on the copper oxide sites can be used to explain this behaviour [10].

The defining of position and sharpness, or width, of the superconducting transition temperature is inconsistent within the literature and is defined many different ways. Different terms are used by these authors, with the most common terms being the onset,

midpoint and zero resistance points as well as the 5%, 10%, 90% and 95% points. Where the experimental curve begins to drop below the extrapolated high-temperature linear behaviour as expressed by Eq 2.11 is considered the onset or 0% point. In this thesis, the T_c values that are cited are the midpoints at which ρ (T) has decreased by 50% below that of the onset point.

$$T = T_c \qquad when \qquad \rho = \frac{1}{2}\rho_{onset} \tag{2.14}$$

Chapter 3

Pulsed Laser Deposition Experimental Layout

3.1 Film Preparation - The Process of Deposition

A high powered laser beam, generally having an energy fluence of ≈ 3 J/cm^2 [4], is directed into a vacuum chamber and directed onto the target material by the laser optics located outside the vacuum chamber as shown in Figure 3.1 below, which gives the general layout of the pulsed laser deposition system used. In this system, the laser shown was

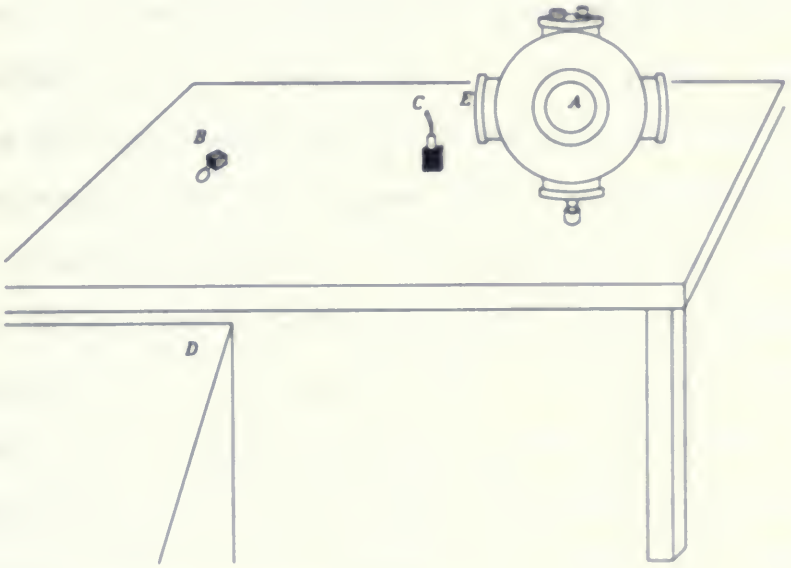

Figure 3.1: **General Layout of PLD System**
A) Window for viewing inside vacuum chamber
B) 45° mirror C) focusing lens
D) excimer laser E) quartz window

a XeCl excimer laser having a wavelength of 308 nm. The laser beam is directed onto a 45° angled mirror, which redirects it through a lens and directed through the window, entering the vacuum chamber at an angle ϕ with respect to the target surface. The parameter of the laser angle of incidence, ϕ, relates to the energy of the ions generated during PLD where the energy of the ions tends to increase as ϕ is increased from 0° to < 90°. This correlation can be attributed to the expected increase in plume adsorption at teh higher incidence angles due to the path length for the laser-plume interactions being proportional to $(\cos\phi)^{-1}$ [2].

3.2 Experimental Design

3.2.1 General Layout

The excimer laser, purchased from McMaster University, was positioned at a 90° angle to the vacuum chamber as can be seen in Figure 3.1. The beam was aligned against the back wall before the mirror was put in place. It was found later that there was a slow leak in the front window of the laser chamber where it had eroded which was affecting the consistency of the beam's intensity. This was solved by polishing the opening for the front window of the laser chamber and replacing the O-ring with a slightly larger one.

The evacuation of the vacuum chamber was a two step process. The system was initially pumped down by a roughing pump to a pressure of $\approx$ 30 mtorr. The chamber to the cryogenic pump was then opened and the cryo pump then evacuated the system over a minimum of 4-5 hour period to a pressure of $\approx 5\text{x}10^{-5}$ torr. This was found to be very time consuming and eventually the cryogenic pump was replaced with a turbo pump which cut the time of the second stage of the evacuation to less than half, while attaining the same pressure.

3.2.2 Target Layout

Each target was prepared using the solid-state method which will be discussed in greater detail in Section 4.2.2 . The targets were affixed to a target holder using a silver epoxy and then the silver epoxy was hardened by heating the target ensemble in an oven at 85 °C for one hour. The target holders were composed of two parts, a small brass disc (approximately 1.5 cm in diameter and 0.3 cm in height) screwed onto a brass pole which was held in place in the gear system by a set screw. The system was designed to hold up to four targets simultaneously, as shown in Figure 3.2, each capable of continuous rotation about its axis throughout the duration of the experiment. A particular target could be rotated into place through an in-plane rotation of the targets via the use of a computer program, a black box relay designed by the electronics shop and a stepper motor. The desired target would be rotated above the heater encasement as shown in Figure 3.2, during the experimental process.

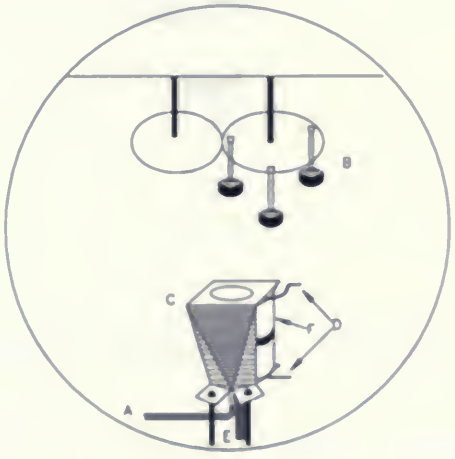

Figure 3.2: **Heater - Target Layout** A: thermocouple B: target-gear ensemble C: heater encasement D: heater wire E: substrate holder F: quartz tube

3.2.3 Heater Design

The heating element was encased within a quartz tube and covered with a stainless steel covering which held the heater in place on three poles in a tri-pod formation within the vacuum chamber. The platinum wire was supplied with a current by an external temperature controller. Eventually the platinum wire was replaced with chromel wire (having a diameter of 18 thousandths of an inch) as the platinum wire when heated would produce "hot spots" along the wire where the current would "build up" and eventually melt the wire through at that spot. To counteract this current build up, the chromel wire was first coiled and then insulated with ceramic beads allowing for the expansion of the wire with increased heat. Figure 3.3 shows the heating element coiled within the quartz tube , the substrate holder was then placed within the heating unit. The temperature of

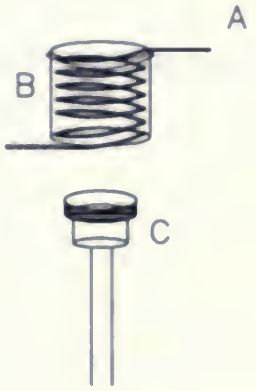

Figure 3.3: **Heater and Substrate Holder**

the heater was controlled externally by a temperature controller. The thermocouple was fixed under the heater - just below the substrate holder. Throughout the duration of the heating process, O_2 gas as a background ambient gas was present and directed over the top of the heating unit by a copper tube, at a partial pressure of approximately 7.501 x 10^{-4} torr (0.100 mbar).

3.3 Pulsed Laser Deposition

As the laser beam enters the vacuum chamber and hits the target, a plume of vapourized material consisting of atoms, molecules and radicals is ablated and collected on the nearby substrate as shown in Figure 3.4. The quartz window where the beam enters

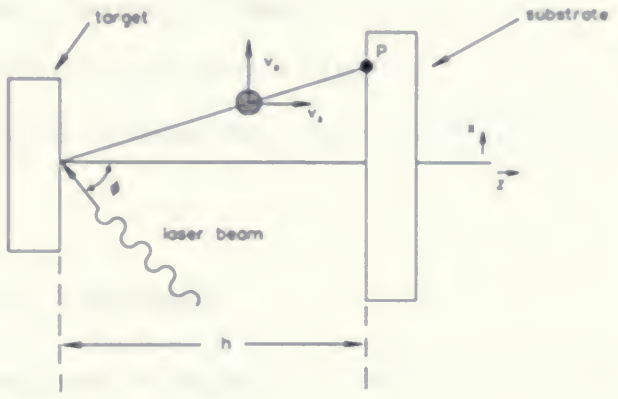

Figure 3.4: **Schematic for Pulsed Laser Deposition**
$\phi \rightarrow$ incident angle of beam on target
$\theta \rightarrow$ effective angle of emission for particles [2]

the vacuum chamber is geometrically shielded from the plume so none of the deposition species coat the inner side of the window during the experiment. A target composed of a porous material results in particulates being ablated more readily and deposited onto the substrate; to alleviate this problem a dense target is used.

3.3.1 Laser Characteristcs

Excimer molecules are formed within a gaseous mixture of their component gases of Xe and HCl in ratios of 36:46 torr respectively, with Ne to bring the gas pressure within the laser chamber to approximately 2890 torr (56 psi). The choice of the laser (whether it be pulsed or continuous wave in nature) is dependent on the specific application - for

evapouration a high power output of the pulsed laser is desired.

For good-quality deposition, the avoidance of hot spots and deviations from a homogeneous uniform laser output is required. This is of particular importance with multicomponent deposition targets since poor beam quality can result in nonstoichiometric films and/or droplet formation. A large absorption coefficient and small reflectivity of the XeCl excimer laser is favoured for the deposition of high T_c superconducting films. Once the laser has been focused properly, for the films to be superconducting, the correct metal composition, crystalline phase and oxygen stoichiometry must be produced in the films.

3.3.2 Stoichiometric Deposition

The deposition rate depends on the pulse repetition rate, and with each pulse of laser energy - localized melting and evapouration occurs leaving a crater in the target. As a means to preserve the stoichiometry in the deposited film, the target is rotated between pulses as each crater created in the target contains resolidified melt with various phases.

Pulsed laser deposition can be described as a three step process:

1. the vapourization of target material
2. the transport of the vapour plume
3. the film growth on the substrate [6].

These steps are repeated thousands of times in a typical run and would fully describe PLD if the target was left unchanged after each pulse. Laser pulses though rarely remove target material in a clean, orderly, layer-by-layer fashion but actually alter the surface both physically and chemically.

A laser pulse induces a rapid thermal cycle in a solid which is dependent on the laser fluence and pulse length, the material's optical absorption coefficient and the thermal properties of the solid such as heat capacity and conductivity. A basic thermal cycle for

one laser pulse is depicted in Figure 3.5. In step a, the laser pulse is absorbed and the

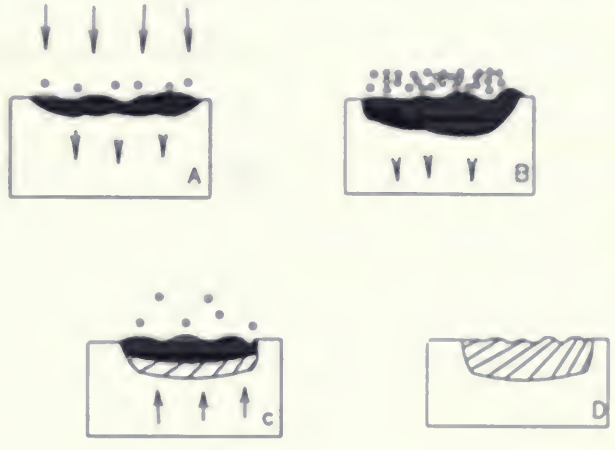

Figure 3.5: **Basic Thermal Cycle**
Schematic of the basic thermal cycle from one laser pulse. [1]

melting and vapourization of the material begins. In b, the melt propagates through the solid and vapourization of the material results. Resolidification of the material begins as is shown by the cross-hatches in c. Finally, resolidification is completed in the solid and the target is ready for the next pulse, d [1].

An increase in laser fluence results in an increase in both the melt depth and the maximum temperature reached within the solid. Low absorption coefficients and high thermal conductivities give a deeper penetration of the thermal pulse into the solid. A shorter pulse length produces a higher melting and solidification velocity.

3.4 Experiemental Considerations

3.4.1 Process Procedure

A clean and highly polished substrate was placed within the system, on the substrate holder and the shield positioned over the top of the heater encasement, shielding the

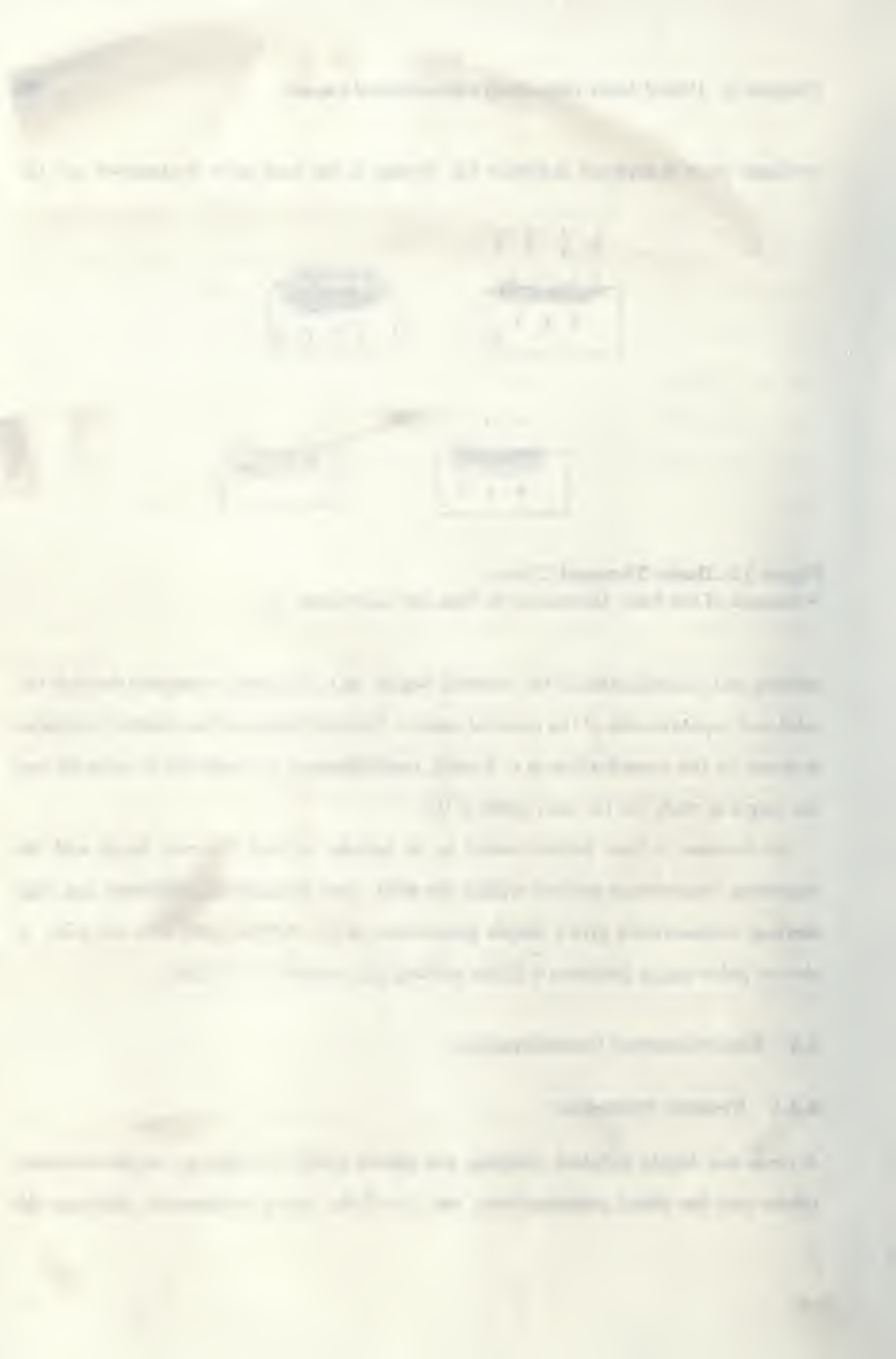

substrate from any debris during the evacuation and heating processes. Once the shiled was rotated into place, the top of the vacuum system containing the targets and their gear system, was placed on top and tightened. The targets, prior to this step, had their srufaces sanded on 600 grit sandpaper to smooth out and clean the surface.

Once the lid is tightened, the system is evacuated to approximately $5x10^{-5}$ torr as previously mentioned in 3.2.1 . During this time, the laser is also rechared. First the old gas is evacuated over a 30-45 min period. Once evacuated, the system is then "flushed" with a high-grade helium, then evacuated again over a 30-45 min period before the gas mixture described in 3.3.1 is used to fill the laser.

After the vacuum chamber has been evacuated, the heating of the substrate is begun. During this heating process, a background gas of oxygen flows continuously and two fans are turned on, one positioned below the chamber and the other above, to keep the chamber from over heating. With the shield still in place 100 pulses of the laser beam are focused onto each rotating target to clean the surface of any carbon contaniments from the sandpaper. When the temperature of the heater was reached, the shield was removed and the deposition process was initiated.

The process of ablation for the deposition of films of alternating layers of YBCO and PrBCO is described in section 3.3. Each layer of YBCO was composed of 4500 pulses, or 1750$\AA$. The PrBCO layers were varied from 1000 to 7000 pulses, or 389 to 2723 $\AA$, and were sandwiched between the YBCO layers. After the layers were deposited, the vacuum chamber was flooded with O_2, bringing it up to atmospheric pressure, and the substrate/film was allowed to cool down to room temperature in the O_2 atmosphere for approximately 45 mins to an hour.

3.4.2 Process Considerations

An optimized laser deposition apparatus is dependent on various factors, beginning with the process parameters relating to the geometry. The substrate was placed below the desired target so that it can readily collect the plume material as the ablated vapour is emitted perpendicular to the target. In a vacuum the thickness deposited per pulse tends to scale approximately with the inverse square of the target - substrate distance h. An increase in the distance h improves film quality, and deposition in the presence of an ambient gas introduces the effects of scattering [2]. For this system, an h $\cong$ 3.6 cm and a pulse rate deposition of $\approx$ 0.3 nm/pulse was found to produce the required stoichiometry.

For the promotion of epitaxial growth in the film, the substrate is heated. The temperature at which the substrate was held during the deposition process was crucial. If the temperature was too high or too low, the uniformity of the film was compromised and with close examination the films could be seen to have pinholes, melts or particulates present.

A temperature gradient existed between the bottom of the substrate holder, where the temperature of the heater was controlled, and the top of the substrate. This difference was measured by a second thermocouple silver epoxied to the top of a substrate and then the heater temperature was systematically raised and stablized. A heater temperature of approximately 820°C was found to produce the most homogeneous films, and at this temperature range a gradient of around 65°C was present.

The deposition of the material in the presence of a constant, low pressure ambient of background gas can both alter the plume properties and change the species mix incident on the growing film. A background gas of O_2 was used to stabilize the desired crystal phase and to prevent decomposition of the oxide film [2]. There is a tendency for a background gas to decrease the efficiency of deposition; the optimum pressure is then

generally the lowest necessary to achieve the desired phase. For this system, an initial background gas pressure of 7.5 x 10^{-4} torr (0.100 mbar) was found to to be sufficient. The use of the background gas throughout the experiment eliminates the need for a post-annealling process.

When all of these parameters are combined, the resulting film has a shiny mirror surface as desired. To ensure that these parameters were acceptable, and consistent, single films of YBCO and PBCO as well as multilayered films of YBCO/PBCO were deposited and their parameters compared to other published results. These results are discussed in more detail in chapter 4.

3.4.3 Film Thickness

To measure the thickness of the deposited film, lithographic patterning was used to achieve a straight and sharp edge between the film and substrate. A drop of resin was first deposited on the center of the film surface. To ensure a light and even distribution of the resin over the film surface, the substrate was taped onto the nozzle of a drill and then rotated at high speed allowing the resin to fan out. Once the resin was distributed, the substrate was then removed from the drill and tape, and a mask was placed on top of the film and resin. It was then exposed to an ultra violet white light for 15 mins, then the film was placed in some developer (mixed in a ratio of 1:1 of developer to distilled water) to develop the exposed portion of the film.

After the film has been developed, it was rinsed under distilled water and allowed to dry. It was then placed in 20 mL of distilled water, and one drop of HCl liquid acid was dropped into the water, removing the developed area of the film. The film was then quickly removed from the dilute HCl solution and again rinsed under distilled water and allowed to dry.

Once patterned, it was placed under a Michelson interferometer and the shift in the

fringe patterns of the film and substrate was measured, see Fig 3.1. The film thickness is then given by:

$$t = \frac{\Delta}{s} \times \frac{\lambda}{2}. \tag{3.1}$$

It was concluded, based on measurements of the deposited films that there was a deposition rate of 3.89 $\mathring{A}$ per pulse.

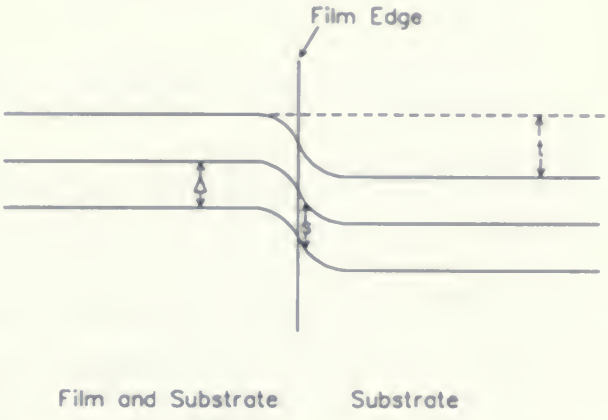

Figure 3.6: **Fringe Pattern**

3.5 Sheet Resistivity and the Four Probe Technique

Resistivity of a typical conductor depends linearly on temperature at high temperatures and obeys the T^5 Bloch law at low temperatures. High temperature superconductors have transition temperatures that are in the linear region. However, the situation is actually more complicated because the resistivity of single crystals of high temperature superconductors is strongly anisotropic [10]. In the case of thin films, the resistance of a square of film between its opposite edges is considered and is known as its "sheet resistivity" where d is the thickness of the film, and A is the cross-sectional area of the

conduction path.

$$R = \frac{\rho L}{A} \tag{3.2}$$

The sheet resitivity is independent of the size of the substrate such that R of a conducting

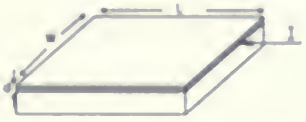

Figure 3.7: **Thin Film - Sheet Resistance**

thin line is proportional just to the number of squares represented by the L/b ratio of the line, where b is the length of the conduction path /citesmith.

A convenient was to measure the dc resistivity of the sample is with the linear four-point probe, as long as the substrate has a high enough ρ so that most of the current I passes through the film. By using a different pair of probes for measuring the voltage drop

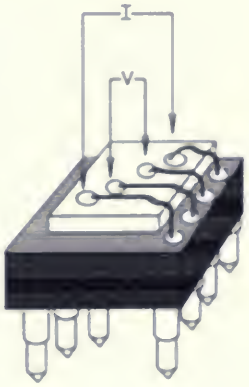

Figure 3.8: **Four Point Contact**

V than the pair used for current flow, the voltage drop B associated with current flow through the contacts is removed from the measurement resulting in only the voltage drop across the distance between two adjacent probes is then measured. Contacts should be

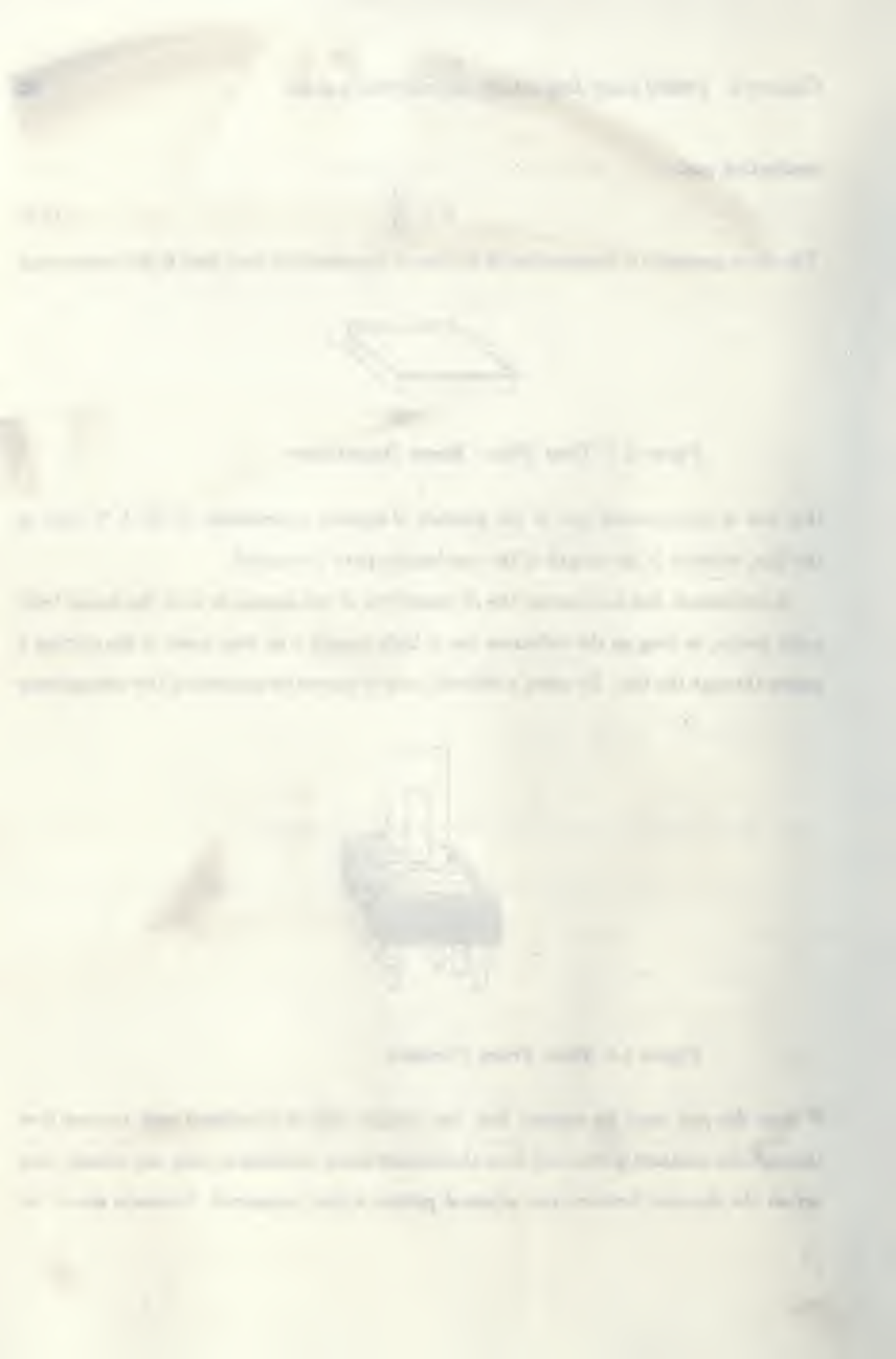

ohmic in nature, and the four-point arrangement makes the quality of the probe contacts non-critical as long as the contacts can pass enough current to generate a measurable V [12].

Chapter 4

Thin Films of High T_c Superconductors

4.1 Superconductivity

4.1.1 Background

Below a characteristic temperature, commonly known as *the superconducting transition temperature, or* T_c, some materials become superconducting. This transition temperature, T_c, can vary from very small values (< 30K), to values above 100K. Above T_c the material is considered to behave like a normal metal. In the normal state, High Temperature Supercondcutors are not particular good conductors, however below T_c they become *perfect* conductors.

The word *superconductivity* refers to the transport of the current through the material, inferring no electrical resistance. A superconductor is a material that exhibits the two characteristic properties of zero electrical resistance and perfect diamagnetism.

4.1.2 Type I vs Type II Superconductors

Initially it was assumed that all superconductors were similar in their behaviour, but in the 1950's there came a general understanding that superconductors actually fell into two classes which are dependent on the sign of the surface energy of the superconducting-normal interface [9].

Nearly all of the pure elemental superconductors studied before 1940 proved to be of Type I with a positive interface energy. They show a reversible first-order phase

transition with a latent heat when the applied field reached a critical field B_c [9]. This field is considered the *intermediate state* where by there is a coexistence of relatively thick normal and superconducting domains running parallel to the field. Their coherence length exceeds their penetration depth so that it is not energetically favourable for boundaries to form between their normal and superconducting phases.

In 1951, Ginzburg & Landry proposed a theory making it possible to calculate the behaviour of superconductors in which the order parameters varied strongly from point to point [9]. This theory accounted for the large magnetic hysteresis of the alloys and their continued superconductivity at fields much greater than the thermodynamic critical field B_c predicted by their heat capacities. From this it became apparent that the alloys were Type II superconductors with a negative interface energy. The penetration depth, λ, is larger than the coherence length, ξ, so it becomes energetically favourable for domain walls to form between the superconducting and normal regions. A Type II superconductor also exhibits zero resistance but has an upper and lower critical field, B_{c2} and B_{c1} respectively. Above B_{c2}, the material behaves normally, below B_{c1} it exhibits perfect diamagnetism and a mixed-type magnetic behaviour and partial flux penetration exists for applied fields between B_{c1} and B_{c2}. Alloys and compounds such as YBCO typically exhibit Type II superconductivity.

4.2 Perovskites & YBCO

A great deal has been written on the high-temperature superconductors being of the perovskite type structure which is held together by electrons that form ionic or covalent bonds between the atoms. All known superconductors having a $T_c > 50K$ are perovskite cuprate superconductors [9], and belong to the perovskite, $CaTiO_3$, crystal structure.

The ideal sturcture for a perovskite compound has the general form of ABX_3, as shown

in Figure 4.1. It takes on a cubic structure, with anion X (typically oxygen) and cation A

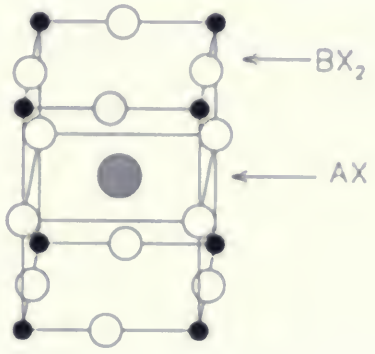

Figure 4.1: **Perovskite Compound**
The perovskite structure ABX_3, Showing the BX_2 planes which correspond to the CuO_2 planes of the cuprate superconductors, and the AX planes, which correspond to the SrO or BaO planes.

having relatively large ionic radii such that they are in contact and therefore determine the size of the structure. Occupying some of the interstices of the A-X network is the B cation that has a smaller radius and forms an octahedron with neighbouring oxygen atoms [9] .

The cuprate superconductors do not have the simple the perovskite structure mentioned above. They are orthorhombic, almost tetragonal materials. Many important features of the perovskite structure are however present in these cuprates. The oxide superconductors replace the Ti^{4+} of the perovskite with Cu^{2+} creating the CuO_2 layering common to the high temperature superconductors. These CuO_2 planes that lie in the a-b plane, exhibit a uniform lattice size and are often adjacent to purely ionic interleaving AX planes such that the O atoms of the interleaving plane coordinate with the Cu atoms of the CuO_2 plane as in the perovskite structure [9], [10] .

A horizontal reflection plane is located at the center and top (and bottom) of the unit cell of the high-temperature superconductor compounds; that is, at a height z on the lower

half of the unit cell, each plane of atoms is duplicated in the upper half. Superconductors that have this reflection plane, but lack end-centering and body-centering operations are called *aligned* because all of their Cu atoms are of one type; either all on the edge, (0,0,z) positions, or all centered, ($\frac{1}{2}$, $\frac{1}{2}$,z), such that they are all located above one another on the same vertical line [10] .

4.2.1 Aligned $YBa_2Cu_3O_7$

Figure 4.2 outlines the location of the atoms and arrangement of the planes for the $YBa_2Cu_3O_7$ unit cell in its orthorhombic form, which superconducts below its transition temperature of $\approx$ 92K.

The YBCO compound can be taken as a stacking of three perovskite units, $BaCuO_3$, $YCuO_2$ and $BaCuO_2$, where two are missing an oxygen which is why c $\simeq$ 3a.

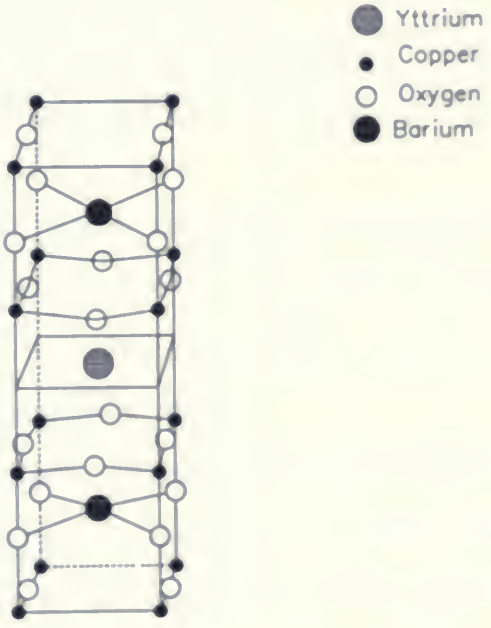

Figure 4.2: **$YBa_2Cu_3O_7$ Crystal Structure**
a = 3.82 Å, b = 3.885 Å, and c = 11.676 Å

Looking closely at the planar structure of YBCO, it is capable of expansion in the c-direction both in the CuO_2 conducting layers and in the interleaved ionic BaO layers. The layering scheme is shown in Fig 4.2 from which it can also be seen that there is puckering in the two CuO_2 planes which sandwich the Y plane. The third copper is contained within the expanded interleaved layers. Varying x in these CuO_x layers alters the doping level of the compound. The CuO_x layer which is often referred to as *chains* of CuO running along the b-direction with no puckering - has a stable structure at low temperatures. Oxygen vacancies sit on these chains. Like the CuO_2 planes, these CuO chains contain free carriers and contribute to the normal conductivity; there is also some evidence that they contribute to the supercurrent [9].

4.2.2 Preparation of YBCO Ceramics

Ceramic tablets of the high temperature superconducting cuprates are generally prepared by the solid-state reaction method described in detail in Table 4.1. This method employs a series of mixing, grinding, and heating cycles with varying temperatures and lengths of heating.

This is a simple method which accounts for its wide usage in the preparation of ceramics. An accurate measurement of the ratios of the materials must be observed and the reagents must be finely ground and thoroughly mixed as particle sizes of a few μm are desired for a dense homogeneous sample.

The YBCO ceramic targets were prepared by mixing the appropriate amounts of Y_20_3, $BaCO_3$, and CuO powders and following the steps outlined in Table 4.1 for the solid-state reaction method. When the YBCO powder reached the forming stage, it was pressed into tablets approximately 2.5 cm in diameter and 0.5 cm in height using a die and press and applying a pressure of 10 tonnes. After the final bake the ceramic target had a density of approximately 5.45 g/cm^3 and a room temperature 2pt resistance of

Table 4.1: Solid State Reaction Method

- Preparation of starting materials (Y_2O_3, $BaCO_3$, CuO giving the molar ratio 1:2:3 for Y:Ba:Cu)
- Mixing (for 2 hours)
- Calcining in Air (for 12 hours at 930°C)
- Pulverizing and mixing (for 2 hours)
- Calcining in air
- Pulverizing and mixing (for 2 hours)
- Calcining in Oxygen atmosphere (for 12 hours at 930°C)
- Pulverizing and mixing (for 2 hours)
- Calcining in Oxygen atmosphere (for 12 hours at 930°C)
- Forming
- Sintering in Oxygen atmosphere (for 24 hours at 950°C)
- Heat treating in Oxygen atmosphere (for 23 hours at 500°C)

[11]

approximately 12 Ω.

4.2.3 $PrBa_2Cu_3O_{7-\delta}$

Following the discovery and structural determination of the 90K $YBa_2Cu_3O_7$ class of superconducting compounds, structurally similar compounds were pursued. One such material shown in Fig 4.3 was $PrBa_2Cu_3O_{7-\delta}$, (PBCO). It is not superconducting or even metallic but is a room-temperature semiconductor and a low-temperature insulator with a-b lattice constants within 1.5% those of YBCO and the same orthorhombic structure as superconducting YBCO [15].

Samples of PBCO were prepared by mixing appropriate amounts of $BaCO_3$, Pr_6O_{11},

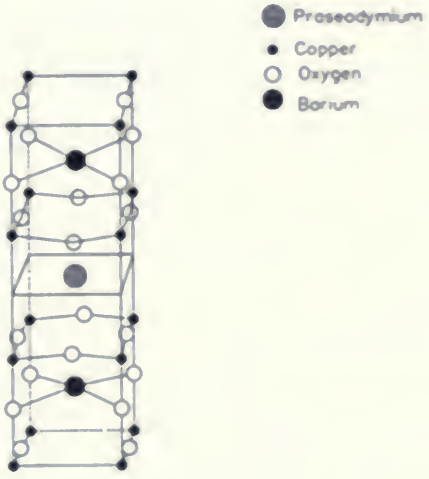

Figure 4.3: **$PrBa_2Cu_3O_7 - \delta$ Crystal Structure**
a = 3.895 Å, and c = 11.648 Å

and CuO powders, which were then subsequently prepared using the solid state reaction method outlined Table 4.1 in the preparation of YBCO. The semiconducting behaviour shown by PBCO allows for the possiblity of varying the interlayer coupling strength of YBCO films by inserting various thickness' of PBCO layers. Consequently,

YBCO/PBCO is an ideal superlattice system for studying anistropy and interlayer coupling effects in YBCO.

4.3 Experimental Results

4.3.1 $YBa_2Cu_3O_{7-\delta}$ Single Films

A single component film of YBCO was intially prepared using pulsed laser deposition with the YBCO target to use as a reference film in two capacities. The first was to optimize the parameters of the system and ensure that it gave good and useable results. And the second was to then use this film as a reference with which to compare the deposited heterostructures. The optimum conditions for the system mentioned in chapter 3 which gave consistently the sharpest superconducting transition where $\Delta T \leq 3K$, and the steepest slope in the metallic state, slope $\leq 0.2\ K^{-1}$, occurred with a heater temperature of approximately 820°C, O_2 partial pressure between 0.1000 mbar and 0.1500

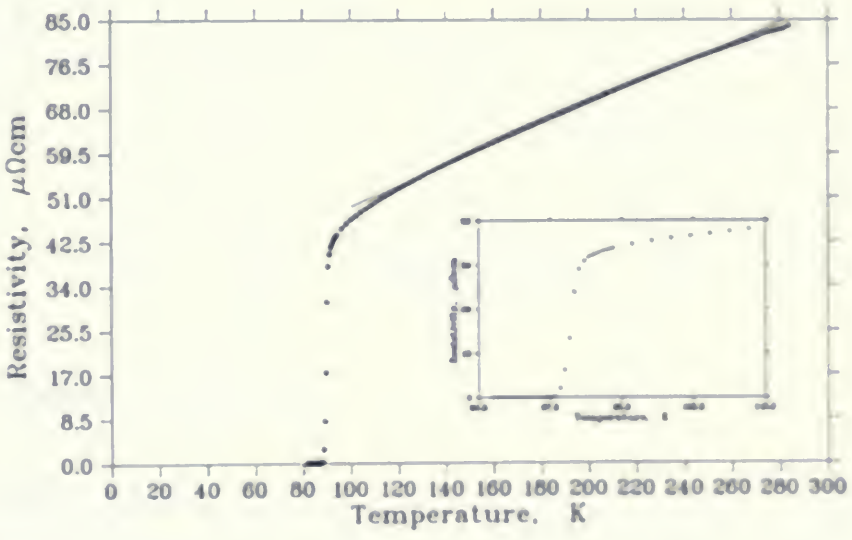

Figure 4.4: $YBa_2Cu_3O_7$

mbar, an angle of incidence of the laser on the target of around 20° and a pulse rate of approximately 2.3 pulse/sec. A YBCO film of thickness 175nm was prepared which had a 4pt room temperature resistance of 1.7 Ω; taking the film thickness into account a room temperature resistivity of 85 $\mu\Omega$cm is found. Figure 4.4 shows the temperature dependence of the resistivity. A conventional linear fit for the normal state of the film is satisfactory, and from Figure 4.4 a T_c of 91K is extrapolated.

4.3.2 $PrBa_2Cu_3O_7$ Single Film

A single component reference film of PBCO was also prepared, using the same parameters and thickness as the YBCO film of Section 4.4.1 . The resistivity shown in Figure 4.5

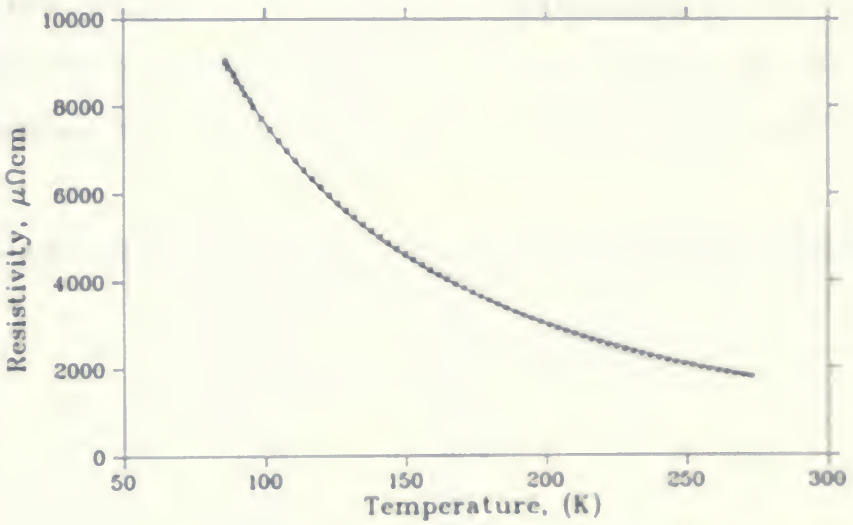

Figure 4.5: $PrB_2Cu_3O_7$

indicates a semiconducting behaviour. As temperature decreases the resistivity of the sample increases such that $\rho(T) \propto \exp(T)$. It can also be seen that the room temperature resistivity of the PBCO film is much higher than that of the YBCO film.

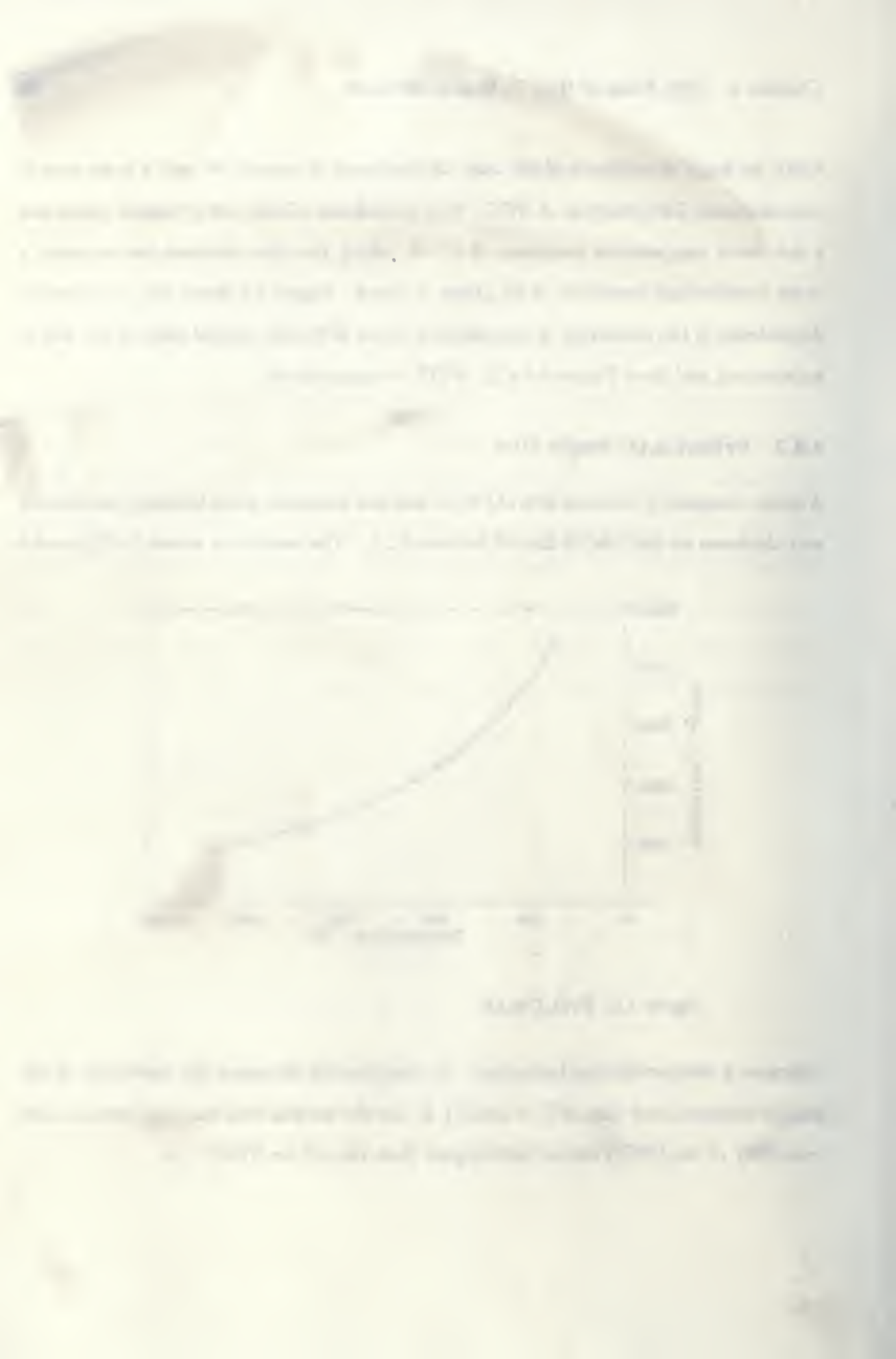

4.3.3 $YBa_2Cu_3O_{7-\delta}/PrBa_2Cu_3O_{7-\delta}$ Superlattices

The thickness of the YBCO layers for all the superlattices was held constant at of 175 nm, while the thickness of the PrBCO layers was varied for each sample from 38.9 nm to 272.3 nm. The superlattices were deposited under the same conditions as those previously used for the YBCO and PrBCO films, alternating the layers of YBCO and PrBCO with a YBCO layer closest to the substrate. Results for some of these superlattices are shown compared to the YBCO film in Figure 4.6.

Comparing first the critical temperatures of the superlattices, summarized in Table 4.2, as the thickness of the PrBCO layers increases there is a slight decrease in the critical temperatures of the superlattices. Li *et al* [17] had previously noted that T_c decreased with increasing thickness of PrBCO or with decreasing thickness of YBCO and attributed this trait to coupling effects in the c-direction between the unit cell layers of YBCO. As summarized in Table 4.2, the T_c of the superlattices prepared for this thesis

Table 4.2: Critical Temperature Values for YBCO/PrBCO Superlattices

Pr Thickness nm	T_c K, ($\pm$ 0.05K)
0 (YBCO)	91.0
58.3	90.9
77.8	90.4
116.7	90.3
155.6	90.2
194.5	89.9
272.3	90.0

remains higher than 89 K in all cases which is a result of the high number of coupled unit cell layers of YBCO. That is, even though the thickness of the PrBCO layers becomes quite large , the YBCO layers are still able to couple strongly. While in the study of Li

et al. the decrease in T_c was found to be more dramatic using thinner layers of YBCO,

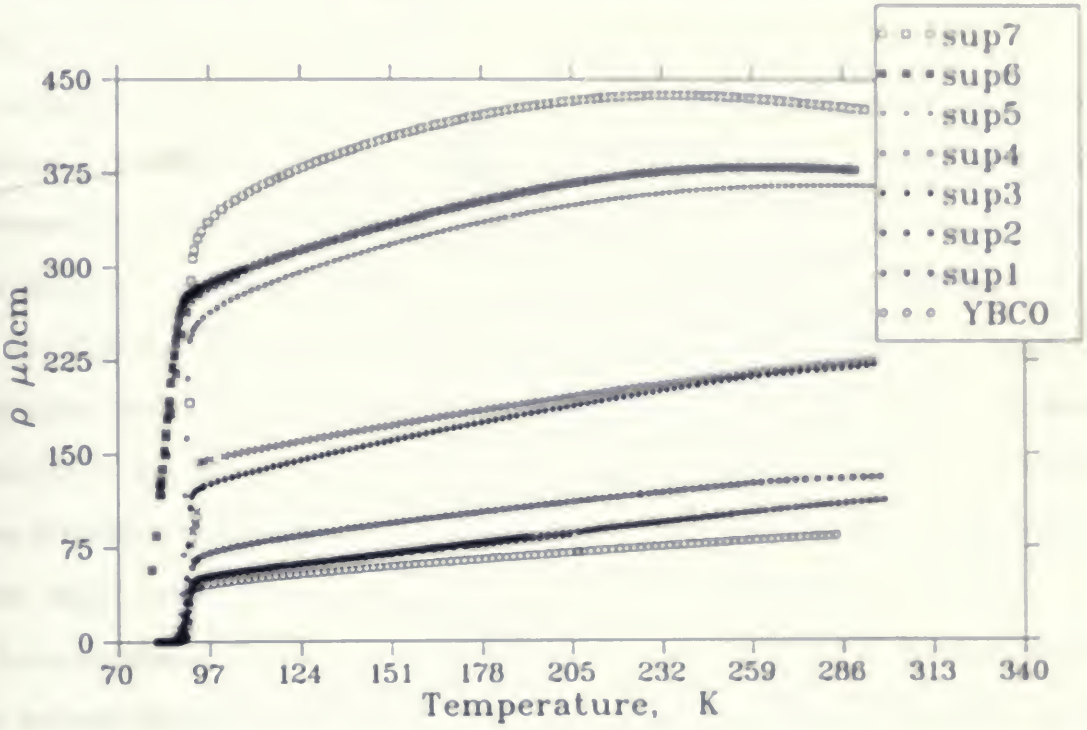

Figure 4.6: **YBCO/PrBCO Superlattice Resistivities** where sup1, sup2, sup3, sup4, sup5, sup6, and sup7 refer to the PrBCO layering thickness' of 58.3nm, 77.8nm, 116.7nm, 155.6nm, 194.5nm, 232.8nm and 272.3nm respectively

in this case the strong coupling between the thicker YBCO layers results in a decrease of the superconducting transition temperature of less than 5K as the PBCO layers varied in thickness from 58.3 nm to 272.3 nm.

An interesting feature of Figure 4.6 is the increase in the resistivity of the film as the thickness of the PrBCO layers is increased. Along with this, there is an apparent positive curvature near 250K for the superlattices with PBCO layer thickness' above 155.6 nm, that becomes more pronounced as the PBCO layer thickness further increases. Solvojov *et. al.* [18] also noticed this effect in very thin films which exhibited a much more pronounced positive curvature for superlattices containing a similar ratio. Additional scattering of charge carriers due to the layer boundaries between the YBCO and PrBCO layers is believed to attribute to the increase in ρ. A pronounced increase in the resistivity occurs fairly steadily with every 64.8 nm increase of the PBCO layer thickness.

Looking again at Fig 4.6 and considering the linear portions of the superlattices before they become superconducting, a linear fit was completed to the regions where they are exhibiting a metallic behaviour. It was noticed that there is an increase in the slope of

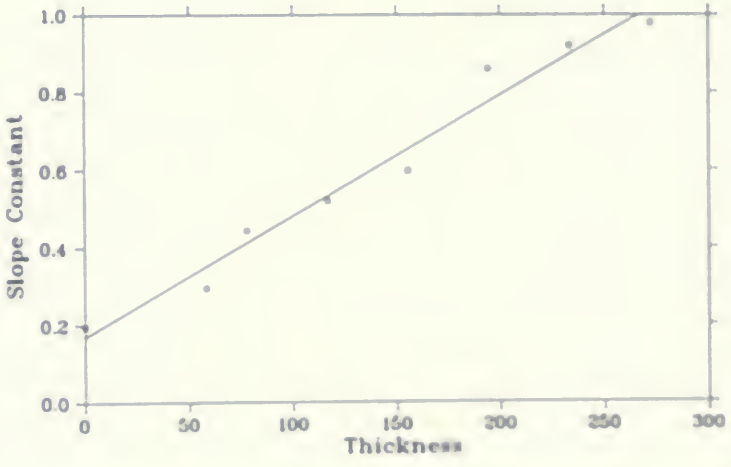

Figure 4.7: **PrBCO Thickness vs Resistivity Slope Constant**

the superlattices with the increasing PrBCO thickness. Figure 4.7 shows that the slope constant exhibits a linear relationship with the thickness of the PrBCO layers.

Chapter 5

Conclusions

A pulsed laser deposition system consisting of a XeCl excimer laser, a vacuum chamber, and a 45° mirror and focusing lens combination for steerin the laser beam was developed. Within the vacuum chamber, a rotating target system, heater and substrate holder were designed. To ensure that the system was operational, thin films of $YBa_2Cu_3O_{7-\delta}$ and $PrBa_2Cu_3O_{7-\delta}$ were deposited from ceramic tablets made using the solid-state reaction method. Using these compounds (YBCO and PrBCO), the conditions within the system were optimized and the resulting films were compared to previously published results. A depositing thickness of approximately 0.38 nm/pulse was consistently found by the use of lithography and a Michelson microscope. The one component $YBa_2Cu_3O_{7-\delta}$ film deposited under optimal conditions had a T_c of 91K and exhibited metallic resistivity above T_c. The one component $PrBa_2Cu_3O_{7-\delta}$ film prepared under these same conditions showed semiconducting behaviour. As a further test of the capabilities of the system, $YBa_2Cu_3O_{7-\delta}/PrBa_2Cu_3O_{7-\delta}$ heterostructures were also deposited under the same conditions. It was found, as expected, that the T_c decreased slightly as the $PrBa_2Cu_3O_{7-\delta}$ layer thickness was increased. Also an increase in the absolute magnitude fo the resistivity was noted as the $PrBa_2Cu_3O_{7-\delta}$ layer thickness increased. Positive curvature in the resistivities above T_c was observed for films with thick PrBCO layers. These results were all in good agreement with those of previously published materials.

The next step in this research would be to continue work on the heterostructures to consider further their resistive nature as the $PrBa_2Cu_3O_{7-\delta}$ layer thickness is further increased.

Bibliography

[1] D.B. Chrisey, G.K. Hubler, *Pulsed Laser Deposition of Thin Films* (John Wiley & Sons, Inc., New York, 1994).

[2] K.L. Saenger *Processing of Advanced Materials* **2**, 1 (1993).

[3] X.D. Wu, T. Venkatesan, A. Inam, X.X. Xi, Q.Li, W.L. Mclean, C.C. Chang, D.M. Hwang, R. Rmaesh, L. Nazar, B. Wilekns, S.A. Schwarz, R.T. Ravi, J.A. Marinez, P.England, J.M. Tarascon, R.E. Muenchausen, S. Foltyn, R.C. Estler, R.C.Dye, A.R. Garcia, and N.S. Nogar *Laser Ablation of Materials Synthesis vol 160* (to be published).

[4] A. Bourdillon, N.X. Tan Bourdillon, *High Temperature Superconductors: Processing and Science* (Academic Press, Inc., San Diego, 1994).

[5] J.G. Bednorz and K.A. Müller *Z. Phys. B* **64**, 189 (1987).

[6] M.K. Wu, J.R. Ashburn, C.J. Torny, P.H. Hor, R. L. Meng, L. Gao, Z.J. Huang, Y.Q. WWWang and C.W. Chu *Phys. Rev Lett.* **58**, 908 (1987).

[7] Z.Z. Sheng and A.M. Hermann, *Nature* **332**, 138 (1988).

[8] A. Shilling, M. Cantoni, J.D. Guo and H.R. Ott, *Nature* **363**, 56 (1993).

[9] J.R. Waldram, *Superconductivity of Metals and Cuprates* (Institute of Physics Publishing, Bristol and Philidelphia, 1996).

[10] C.P. Poole Jr., H.A. Farach, R.J. Creswick, *Superconductivity* (Academic Press, Inc., San Diego, 1995).

[11] A.C. Vajpei and G.S. Upadhyaya, *Powder Processing of High T_c Oxide Superconductors* (Trans Tech Publications Ltd, Brookfield, 1992).

[12] Donald L. Smith,, *Thin-Film Deposition Principles & Practice* (McGraw-Hill Inc., New York, 1995).

[13] Kasturi L. Chopra, *Thin Film Divce Applications* (Plenum Press, New York, 1983).

[14] Robert F. Pierret, *Modular Series on Solid State Devices, Volume 1 - Semiconductor Fundamentals* (Addison-Wesley Publishing Company, Massachusetts, 1983).

[15] Douglas H. Lowndes, David P. Norton, and J.D. Budai *Physical Review Letters* **65**, 1160 (1990).

[16] Bin Okai, Koh Takahashi, Hiroshi Nozaki, Masanobu Saeki, Michikazu Kosuge and Masatsune Ohta *Japanese Journal of Applied Physics* **26**, L1648, (1987).

[17] Q. Li, X. Xi, X.D. Wu, A. Inam, S. Badlamannati, and W.L. McLean *Physical Review Letters* **64**, 3086 (1990).

[18] A.L. Solovjov, H.U. Habermeier, and I.E. Trofimov *Physica B* **199-200** 260 (1994).

[19] B. Okai, K. Takahashi, H. Nazaki, M. Saeki, M. Kosuge and M. Ohta *Japanese Journal of Applied Physics*, **26** L1648 (1987).

[20] S. Chittipeddi, Y. Song, D.L. COx, J.R. Gaines and J.P. Golben *Physical Review B* **37** 7454 (1988).

[21] H.U. Habermeier, A.L. Solovjov and V.B. Dmitriev, *Physica C* **235-240** 1959 (1994).

[22] C.A. Hollin, S.W. Goodyear, N.G. Chew, R.G. Humphreys, and J.S. Abell *Physica C* **235-240** 721 (1994).

[23] Q. Li, C. Kwon, X.X. Xi, S. Bhattacharya, A. Walkenhorst, T. Venkatesan, S.J. Hagen, W. Jiang and R.L. Greene *Physica B* **194-196** 2389 (1994).

[24] D.B. Haviland, Y. Liu, and A.M. Goldman *Physical Review Letters* **62** 2180 (1989).

[25] B.R. Zhao, X.G. Qui, S.Q. Guo, J.L. Zhang, P. Xu, Y.Z. Zhang, Y.Y. Zhao and L. Li *Physica C* **204** 341 (1993).

[26] I.E. Trofimov, D.H. Leach, A.P. Litvinchuk, K. Kamaras, C. Thomsen, H.U. Habermeier and M. Cardona *Physica C* **209** 51 (1993).

[27] R.F. Wood *Physical Review Letters* **66** 829 (1991).

[28] C.M. Fu, V.V. Moshchalkov, E. Rosseel, M. Baert, W. Boon, and Y. Bruynseraede *Physica C* **206** 110 (1993).

[29] V.V. Metlushko, G. Güntherodt, B.B. Moshchalkov, C.M. Fu, Y. Bruynseraede, G. Jakob, T. Hahn and H. Adrian *Physica B* **194-196** 2391 (1994).

[30] G. Liu, G. Xiong, G. Li, G. Lian, K. Wu, S. Liu, J. Li, and S. Yan *Physical Review B* **49** 15 287 (1994).

[31] J. Li, K. qi Luo, and C. de Gong *Applied Physics Letters* **64** 3329 (1994).

[32] M. Affronte, J.M. Trisone, O. Brunner, L. Antognazza, L. Mieville, M. Decroux and O Fisher *Physical Review B* **43** 11 484 (1991).

[33] Y. Matsuda, A. Fujiyama, S. Komiyama, T. Terashima, K. Shimura and Y. Bando *Physica C* **185-189** 2055 (1991).

[34] R.K Singh *Journal of Non-Crystalline Solids* **178** 199 (1994).

[35] T. Benkatesan, X.D. Wu, A. Inam, and J.V. Wachtman *Applied Physics Letters* **52** 1193 (1988).

[36] S.D. Chen, S.Y. Lee, J.P. Golben, S.I. Lee, R.D. McMichael, Y. Song, T.W. Noh, and J.R. Gaines *Review of Scientific Instrumentation* **58** 1565 (1987).

[37] Z.X. Shi, H.L. Ji, X. Jin, X.X. Yao, X.S. Rong, X.G. Qui and Z. Li *Physica C* **215** 439 (1993).